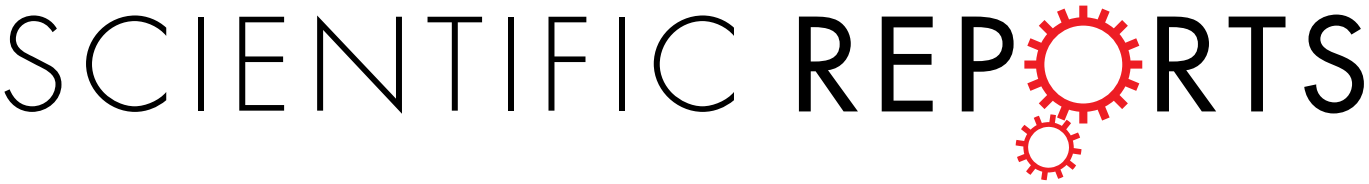

OPEN

Rational Construction of Uniform CoNi-Based Core-Shell Microspheres with Tunable Electromagnetic Wave Absorption Properties

Received: 20 October 2017
Accepted: 12 January 2018
Published online: 16 February 2018

Na Chen[1,2], Jian-Tang Jiang[1], Cheng-Yan Xu[1,2], Shao-Jiu Yan[3] & Liang Zhen[1,2]

Core-shell particles with integration of ferromagnetic core and dielectric shell are attracting extensive attention for promising microwave absorption applications. In this work, CoNi microspheres with conical bulges were synthesized by a simple and scalable liquid-phase reduction method. Subsequent coating of dielectric materials was conducted to acquire core-shell structured CoNi@TiO_2 composite particles, in which the thickness of TiO_2 is about 40 nm. The coating of TiO_2 enables the absorption band of CoNi to effectively shift from K_u to S band, and endows CoNi@TiO_2 microspheres with outstanding electromagnetic wave absorption performance along with a maximum reflection loss of 76.6 dB at 3.3 GHz, much better than that of bare CoNi microspheres (54.4 dB at 17.8 GHz). The enhanced EMA performance is attributed to the unique core-shell structures, which can induce dipole polarization and interfacial polarization, and tune the dielectric properties to achieve good impedance matching. Impressively, TiO_2 coating endows the composites with better microwave absorption capability than CoNi@SiO_2 microspheres. Compared with SiO_2, TiO_2 dielectric shells could protect CoNi microspheres from merger and agglomeration during annealed. These results indicate that CoNi@TiO_2 core-shell microspheres can serve as high-performance absorbers for electromagnetic wave absorbing application.

Electromagnetic wave absorbing (EMA) materials have attracted much attention in past few decades because of the increasing requirement for conquering the electromagnetic interference and electromagnetic disclosure[1–5]. EMA materials with wide absorption bands, strong reflection loss and satisfactory weather resistance are urgently required[6–9]. A variety of materials have been explored for using as EMA fillers. Ferromagnetic metal/alloy particles, such as CoNi particles, attract considerable interest as microwave absorbers due to their unique ferromagnetic features, including high saturation magnetization, high Snoek's limit, and high magnetocrystalline anisotropy[10,11]. For CoNi particles, the EMA performance is strongly influenced by the particle morphology and microstructure[12]. Great efforts have been devoted to design and synthesize CoNi particles with various shapes, such as nanoparticles[13], microspheres[14], chains[15,16], wires[17,18], flowers[19–21], nanotubes[22,23] and nanoleaves[24]. These studies preliminarily investigated the effects of morphology on EMA properties via the application of CoNi particles, and confirmed that size and shape of particles had an obvious effect on EMA performance. Specially, according to the electromagnetic wave propagation theory, the modified surface could effectively tailor the EMA performance through surface scattering effects[12]. However, systematic investigation focusing on the impacts of configuration and surface morphology on the electromagnetic properties is scarce. Additionally, CoNi materials usually suffer from ease of oxidation, resulting in limited practical applications.

To fabricate core-shell structured composite particles that integrate the ferromagnetic components and dielectric components together at sub-micro/nano scales is believed to be a promising approach to solve the above problems[25,26]. The protecting shells on particles' surface yield multiple interfaces and isolates particles

[1]School of Materials Science and Engineering, Harbin Institute of Technology, Harbin, 150001, China. [2]MOE Key Laboratory of Micro-System and Micro-Structures Manufacturing, Harbin Institute of Technology, Harbin, 150080, China. [3]Beijing Institute of Aeronautical Materials, Beijing, 100095, China. Correspondence and requests for materials should be addressed to J.-T.J. (email: jjtcy@hit.edu.cn) or L.Z. (email: lzhen@hit.edu.cn)

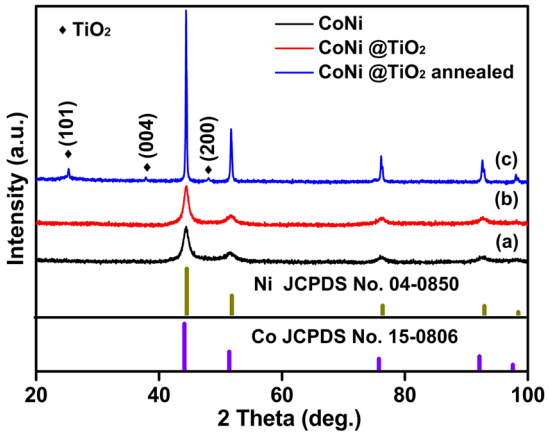

Figure 1. XRD patterns of (**a**) as-prepared CoNi microspheres, (**b**) CoNi@TiO_2 core-shell microspheres and (**c**) CoNi@TiO_2 core-shell microspheres annealed at 600 °C.

from contacting each other, which contributes to the dielectric dissipation[27], suppresses eddy current[28] and also avoids decay-induced performance degradation. Improved EM properties, either in amplitude or in spectrum characteristics, were observed in this catalog of composite materials, suggesting the great potential of core-shell composite structures[29–31]. For example, Zhang *et al*. synthesized core-shell Ni-TiO_2 composite microspheres with enhanced microwave absorption properties, which arises from multiple interfacial polarization and high thermal conductivity of rutile TiO_2[32]. Ren *et al*. fabricated three-dimensional SiO_2@Fe_3O_4 core-shell nanorods array/graphene architecture. The significantly improved dielectric loss of SiO_2@Fe_3O_4 composite is attributed to the dipolar polarization and interfacial polarization[33]. Li *et al*. successfully prepared FeCo/graphene hybrids with remarkable improvement in permeability and permittivity, which leads to remarkable enhancement in EM absorption properties[34].

Among numerous dielectrics shell materials, including carbon materials, SnO_2, $BaTiO_3$, TiO_2, SiO_2 as well as polymers, TiO_2 as an important semiconductor material[35–37] has been widely explored for electromagnetic wave absorption applications due to its dominant dipolar polarization and corresponding relaxation phenomena, which contributes to the dielectric loss mechanism[38,39]. Meanwhile, TiO_2 is also attractive as a coating material to enhance the microwave absorption performance since it owns high dielectric constant[40]. Accordingly, it is expected that the interface between the magnetic core and TiO_2 shell could produce some intriguing interactions, which could extremely enhance EMA properties of ferromagnetic particles.

The purpose of this work was to design and fabricate core-shell composites to achieve materials with outstanding EMA performance. A facile and efficient method was developed to prepare composite microspheres with CoNi as cores and TiO_2 as shells, in which CoNi cores can contribute to the magnetic loss, while TiO_2 shells can contribute to the dielectric loss. The microwave absorption properties of CoNi microspheres and core-shell composites microspheres were evaluated. The results suggest that CoNi@TiO_2 microspheres possess outstanding microwave absorption capabilities. Our findings give insights into the understanding of the effects of core-shell structure on the microwave absorption performance, which can be extended to other ferromagnetic metals and ferrites for EMA applications.

Results and Discussion

The crystal structure of as-prepared CoNi microspheres and core-shell structure composites were characterized by XRD. As shown in Fig. 1a, four strong peaks ($2\theta = 44.4°$, 51.6°, 76.3° and 92.7°) are observed in the XRD pattern, which can be indexed to the (111), (200), (220) and (311) planes of face-centered cubic (*fcc*) phase CoNi[41], respectively (JCPDS no. 15–0806 for *fcc* Co, JCPDS no. 04–0850 for *fcc* Ni). No other characteristic peaks are observed in the pattern, indicating the high purity of as-obtained CoNi microspheres. The characteristics peaks of TiO_2 cannot be detected in the XRD pattern of as-synthesized CoNi@TiO_2 (Fig. 1b), suggesting that the TiO_2 shells should be amorphous. After annealed at 600 °C for 2 h, three characteristic diffraction peaks were found to be located at 2θ of 25.3°, 37.8° and 48.0°, corresponding to the (101), (004) and (200) crystal planes of anatase TiO_2 (JCPDS No. 21–1272), as shown in Fig. 1c. Meanwhile, XRD peaks of annealed microspheres are much sharper and stronger, demonstrating the improvement of crystallinity for CoNi@TiO_2 microspheres. The crystal structure of CoNi@SiO_2 microspheres were also characterized by XRD (Fig. S1). No characteristic peaks corresponding to crystalline SiO_2 can be detected in the XRD patterns, indicating that SiO_2 shells should be amorphous states.

The morphology of CoNi microspheres was observed by SEM and TEM. SEM image in Fig. 2a and TEM image in Fig. 2c reveal that the as-prepared CoNi particles are uniform microspheres with an average diameter of about 300 nm. Interestingly, it can be observed that conical bulges with a length of 5–15 nm emerge on the pristine CoNi microspheres, as shown in Fig. 2b and d. Energy dispersive X-ray spectroscopy (EDS) analysis was performed to check the compositions (Fig. S2). The atomic ratio of Co/Ni (50.2:49.8) is approximately 1:1, very close to the stoichiometry of CoNi. Element mappings obtained from EDS analysis also suggest that the distribution of Co and Ni elements is rather homogeneous in entire microsphere. High-resolution TEM (HRTEM)

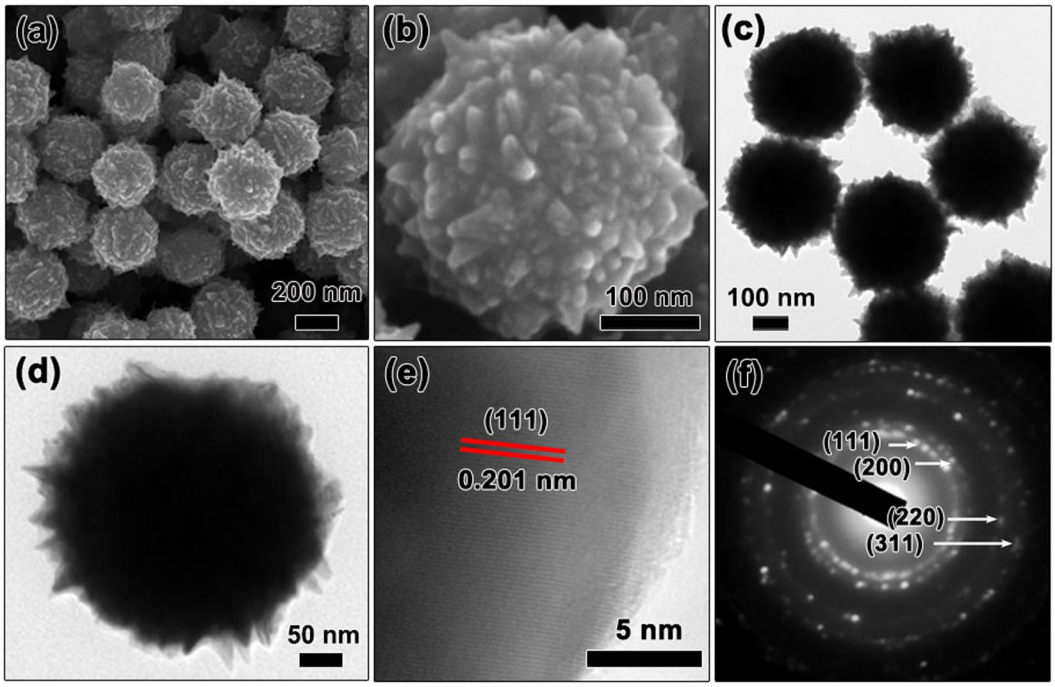

Figure 2. Characterization of as-synthesized CoNi microspheres. (**a**,**b**) SEM images; (**c**,**d**) TEM images; (**e**) HRTEM image; (**f**) SAED pattern.

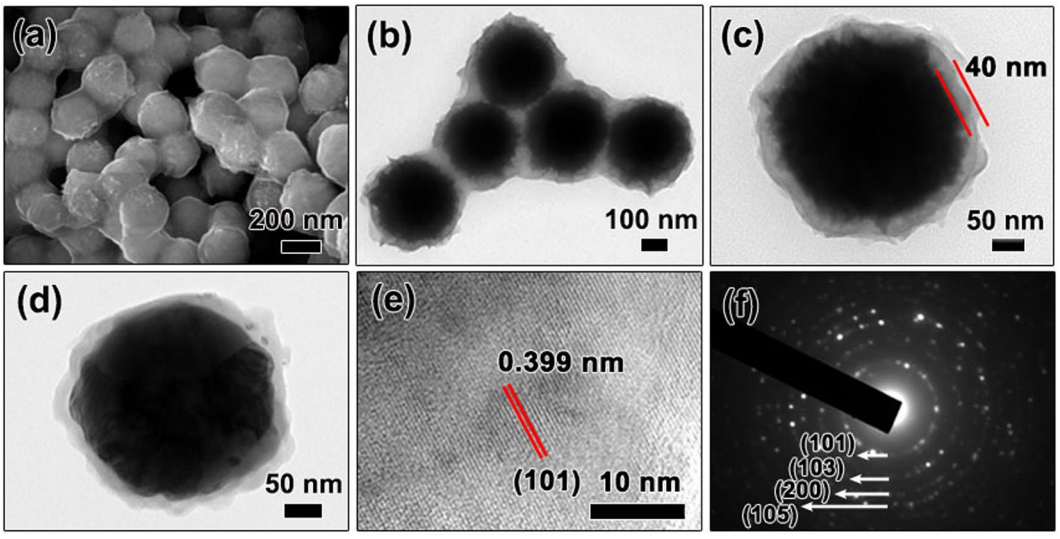

Figure 3. Characterization of the structure and morphology of CoNi@TiO_2 core-shell microspheres. (**a**) SEM and (**b**) TEM image of as-prepared CoNi@TiO_2 microspheres. (**c**) TEM image of a single CoNi@TiO_2 microsphere. (**d**) TEM image of CoNi@TiO_2 microsphere annealed at 600 °C. (**e**) HRTEM image and (**f**) SAED pattern of TiO_2 shell after annealed.

image taken from a single microsphere reveals the well-resolved lattice fringes corresponding to the (111) plane ($d = 0.201$ nm) of cubic CoNi, as described in Fig. 2e. Selected-area electron diffraction (SAED) pattern depicted in Fig. 2f shows distinct diffraction rings corresponding to (111), (200), (220) and (311) crystallographic planes of cubic CoNi, in accordance with XRD analysis. HRTEM and SAED results clearly prove the highly crystalline of CoNi microspheres. Based on SEM and TEM analysis, it is confirmed that CoNi microspheres with conical bulges surface have been successfully fabricated via liquid phase reduction method. The unique and novel conical bulge of CoNi microspheres is expected to enhance EMA performance.

CoNi microspheres are coated by TiO_2 shells through a sol-gel method. The microstructure and morphology of CoNi@TiO_2 composites microspheres were characterized by SEM and TEM. SEM and TEM images in Fig. 3a,b show the uniform size distribution and core-shell structure of CoNi@TiO_2 composites particles. The microsphere

morphology characteristics of CoNi could be well maintained after TiO_2 coating. It is worth noting that some conglomerates containing a few CoNi@TiO_2 microspheres are observed, as shown in Fig. 3a. CoNi microspheres are supposed to aggregate together when wrapped in TiO_2 during the sol-gel process, leading to the slender shape and close-packed microstructure of these conglomerates (Fig. 3b). The intervals between CoNi particles are 10–50 nm, which enable the local conducting within the conglomerates. The EDS spectrum as well as elemental mappings obtained from an individual CoNi@TiO_2 microsphere in Fig. S3 confirms homogeneous distribution of Co, Ni, O and Ti elements. From the high-magnification SEM image in Fig. S3b, it could be clearly seen that the surface of CoNi@TiO_2 is different from that of CoNi microsphere. The core-shell microspheres have a nearly flat surface, indicating that TiO_2 shell covers the surface of CoNi particles. TEM image in Fig. 3c verifies the typical core-shell structure of CoNi@TiO_2, in which an outer layer of about 40 nm in thickness can be clearly distinguished. SEM image in Fig. S4 shows that the morphology of CoNi@TiO_2 microspheres was well retained after annealed at 600 °C. The sizes of CoNi core exhibit negligible change and the thickness of TiO_2 shell remains to be about 40 nm (Fig. 3d). The corresponding HRTEM image taken from TiO_2 shell of a single annealed microsphere is exhibited in Fig. 3e. The lattice fringe with distance of 0.399 nm is in good accordance with the (101) plane of anatase TiO_2. SAED pattern of TiO_2 shell in Fig. 3f confirms that TiO_2 is typical anatase phase with diffraction rings corresponding to the (101), (103), (200) and (105) planes, respectively. These results suggest that coating of CoNi microspheres with TiO_2 shells could be successfully carried out by using a sol-gel method, and the annealing at high temperature (see XRD pattern in Fig. S5 and associated discussion in Supporting Information) can effectively tailor the crystal structure of TiO_2 layers. More importantly, TiO_2 shells can effectively protect and isolate CoNi microspheres from merger and aggregation in high-temperature annealing process.

SiO_2 is also extensively used as a coating material since it is a good insulator. Our previous study indicated that the EMA properties of Co_7Fe_3 nanospheres could be improved by introduced SiO_2 shells[42]. The morphology of as-obtained CoNi@SiO_2 microspheres is rather uniform, as shown in Fig. S6. Elemental mappings obtained from EDS analysis (Fig. S7) reveal the homogeneous distribution of Co, Ni, O and Si elements. A close observation in Fig. S6c presents that the outcrop of conical bulges become blunt, revealing that SiO_2 was successfully deposited onto CoNi surfaces. TEM image in Fig. S6d confirms that the SiO_2 shell on the surface of CoNi microspheres is about 30 nm in thickness. The spherical morphology of CoNi@SiO_2 was retained after annealed at 600 °C, however, the microspheres tend to merge and agglomeration is observed at local regions, as shown in Fig. S6e and f. The merging and resulted agglomeration of CoNi@SiO_2 microspheres during annealing may cause the decrease of dielectric properties. These results suggest the TiO_2 coating could protect CoNi microspheres from merger and agglomeration during annealed process more effectively compared with SiO_2 coating. In the process of annealing, the difference of microstructure evolution between CoNi@TiO_2 and CoNi@SiO_2 should have a different effect on EMA performance. On the basis of above SEM and TEM analysis, it is confirmed that core-shell structure CoNi@TiO_2 composites microspheres with TiO_2 shells can be obtained through sol-gel process. It could be deduced that this unique core-shell structure is helpful to improve the EMA performance, which will be discussed in the following part.

The surface compositions and element valence of CoNi and CoNi@TiO_2 microspheres were investigated by XPS, and the results were shown in Fig. 4. The survey spectrum of CoNi microspheres in Fig. 4a reveals that the existence of Co, Ni, O and C elements. To further investigate the chemical states of Co and Ni elements, high resolution XPS spectra were conducted. Fig. 4b shows the high-resolution XPS spectrum of Ni 2p region. The peaks at 852.6 and 870.3 eV can be assigned to Ni $2p_{3/2}$ and Ni $2p_{1/2}$, suggesting the zero valent Ni[11]. The satellite peaks in the spectrum indicated the surface oxidation of nickel. Co 2p XPS spectrum in Fig. 4c shows two primary peaks at 777.8 eV (Co $2p_{3/2}$) and 793.3 eV (Co $2p_{1/2}$) corresponding to metallic cobalt[43], along with satellite peaks at the higher binding energy region. These features belong to the characteristics of Co^{2+}, implying the partial oxidation of cobalt. The presence of oxides cannot be detected by XRD measurement, suggesting their quite low percentage composition.

The survey spectrum of CoNi@TiO_2 in Fig. 4a depicts the existence of Co, Ni, O, C and Ti elements, in agreement with the EDS results. High-resolution XPS spectrum of Ti 2p is shown in Fig. 4d. The peaks at 457.8 eV and 463.7 eV are assigned to Ti $2p_{3/2}$ and Ti $2p_{1/2}$, revealing the formation of TiO_2 on the surface. The survey spectrum of CoNi@SiO_2 in Fig. S8a demonstrates the presence of Co, Ni, O, C and Si elements. The peak at 103.5 eV in Fig. S8b is ascribed to Si 2p, indicating the formation of SiO_2 on the surface. Based on the results of XPS, it can be concluded that CoNi microspheres were achieved and a thin surface layer were oxidized. TiO_2 could be successfully coated on the surfaces of CoNi microspheres to form core-shell structure composite microspheres.

The magnetic properties of CoNi and CoNi@TiO_2 microspheres were measured on a VSM at room temperature, and the results are shown in Fig. 5. The saturation magnetization (M_s), and coercivity (H_c) of CoNi microspheres, CoNi@TiO_2 and CoNi@TiO_2 annealed are compared in Fig. 5b. The saturation magnetization of CoNi microspheres is 98.4 emu/g, about 12.1% lower than that of bulk CoNi (112 emu/g)[24], which may be attributed to the surface oxidation, impurities and defects[10,25]. H_c of CoNi microspheres is 107.0 Oe. The M_s and H_c of CoNi@TiO_2 are 79.6 emu/g and 111.0 Oe, respectively, which are slightly lower than those of CoNi microspheres. The decline of M_s is mainly attributable to the presence of nonmagnetic TiO_2[11]. After annealed at 600 °C, M_s increases to 94.3 emu/g (Fig. 5b), owing to the elimination of crystal defects and improvement of crystallinity. The increase in M_s is beneficial to the improvement of permeability.

The EMA properties of coating are highly dependent on its EM parameters. Fig. 6 shows the frequency dependences of permittivity (ε) and permeability (μ) of specimens containing CoNi and CoNi@TiO_2 as fillers. As for CoNi-based sample (Fig. 6a), ε' does not decline apparently as the frequency increase, while ε'' increases gradually from 0.3 to 2.5 in 2–16 GHz, before decreases to 1.8 at 18 GHz, revealing mild dielectric relaxation in 9–16 GHz band. Compared with CoNi-based specimen, the ε' and ε'' of specimen containing CoNi@TiO_2 as fillers are obviously higher all through the frequency range. For instance, ε' increases from 6.4 to 12.7, and ε'' increases from 0.6 to 2.2 at 6 GHz, as shown in Fig. 6a. Meanwhile, the relaxation becomes intense after TiO_2

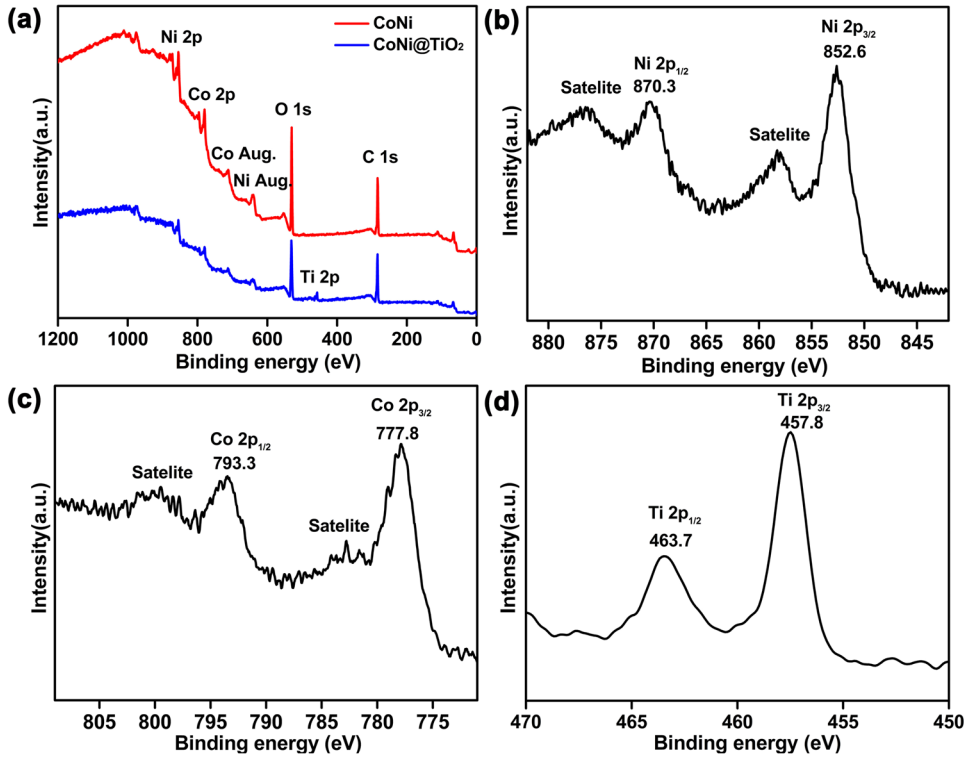

Figure 4. (**a**) XPS survey spectra of CoNi and CoNi@TiO_2 microspheres. High-resolution XPS spectra of (**b**) Ni 2p and (**c**) Co 2p in as-prepared CoNi microspheres. (**d**) High-resolution XPS spectrum of Ti 2p in CoNi@TiO_2 microspheres.

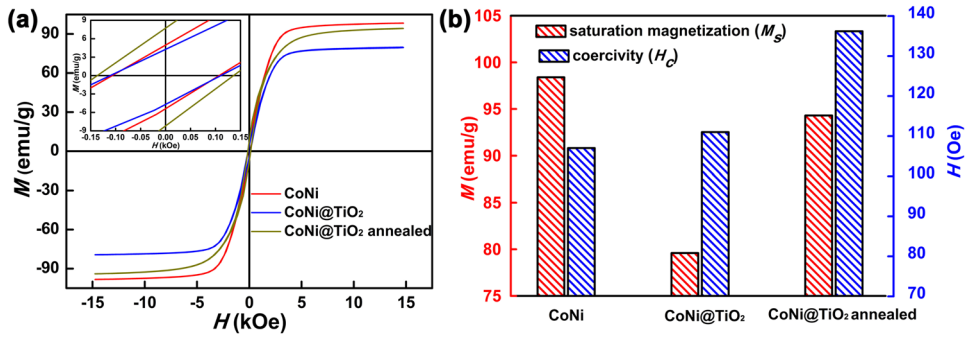

Figure 5. (**a**) Hysteresis loops of CoNi, CoNi@TiO_2 and annealed CoNi@TiO_2 microspheres measured at room temperature. The inset is an enlarged view of the hysteresis loops. (**b**) Magnetic properties of CoNi, CoNi@TiO_2 and annealed CoNi@TiO_2 microspheres.

coating. After annealed at 600 °C, the permittivity of CoNi@TiO_2 further increased. For example, ε' increases from 12.4 to 20.6, and ε'' increases from 0.6 to 1.8 at 2 GHz. Moreover, the dielectric relaxation enhances apparently and shifts to 2–12 GHz. As is well known, the permittivity refers to materials' polarizability, which mainly derives from the interface and dipolar polarizability at microwave frequency[44]. In this case, the evident increase in permittivity is attributed to the enhanced interfacial polarization and the developed dipole polarization. The interfacial polarization arises from the migration of charge carriers on conducting/insulating interfaces according to the Maxwell-Wagner-Sillars theory[45,46]. In this work, CoNi particles dispersed in the paraffin matrix work as charge centers, which can conduce to permittivity on account of interfacial polarization. The coating of TiO_2 on CoNi microspheres introduces metal/dielectric interfaces and increases the interfacial amount, which would improve interfacial polarization and then promote the permittivity, ultimately, enhance the dielectric loss[47]. During TiO_2 coating process, the microspheres aggregated together to generate conglomerates of a slender shape. These elongated conglomerates can be considered as a system of dipoles which can induce intense dipole polarization, leading to the enhancement of permittivity[48]. Additionally, the conductivity of CoNi@TiO_2 microspheres can increase greatly as the defects in the particles eliminates and the crystalline integrity improves during annealing[49]. The improved conductivity is helpful to enhance dielectric relaxation and dipole polarization, leading to

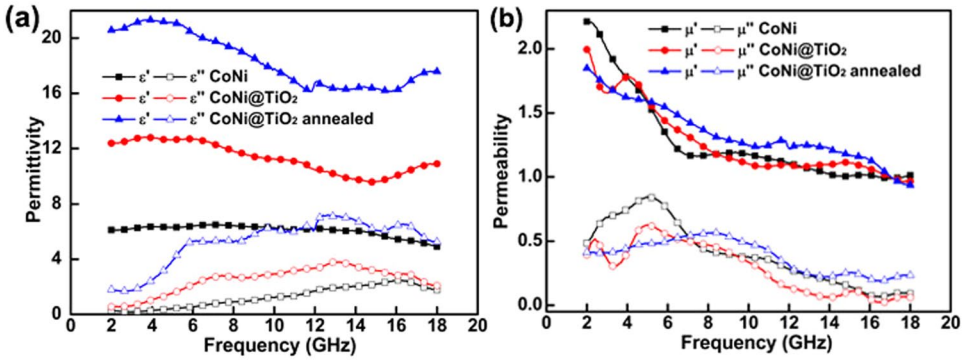

Figure 6. The frequency dependence of (**a**) permittivity and (**b**) permeability for CoNi and CoNi@TiO_2 microspheres.

the evidently increased permittivity of annealed samples. The enhanced permittivity is believed to be beneficial for the improvement of the dielectric loss and electromagnetic absorption performance[27,50]. Furthermore, the enhanced conductivity could cause conductive loss[51], which is also beneficial to improve the electromagnetic wave absorption performance of CoNi@TiO_2 microspheres.

The electromagnetic parameters of CoNi@SiO_2 were also measured for comparison. Fig. S10a shows the ε' and ε'' as a function of frequency for CoNi@SiO_2 microspheres in the range of 2–18 GHz. ε' together with ε'' increase obviously in the whole frequency range after SiO_2 coating, similar to that observed in case of TiO_2 coating. However, the permittivity of specimen drops evidently after the filled CoNi@SiO_2 is annealed, which is quite different from that in CoNi@TiO_2 microspheres. Compared with the specimens containing CoNi@TiO_2 microspheres as fillers, both ε' and ε'' of CoNi@SiO_2 are much lower especially when the annealed fillers are applied. For instance, ε' and ε'' are 17.7 and 6.3 for specimens containing annealed CoNi@TiO_2, 6.0 and 0.7 for specimens containing annealed CoNi@SiO_2 in 10 GHz, respectively. The interface areas and conductivity dominate dielectric relaxation frequency and intensity, and then administrate the permittivity. The significantly decreased permittivity of CoNi@SiO_2 annealed microspheres can be ascribed to the reduced interface areas. The well-dispersed CoNi@SiO_2 microspheres tend to merge together to form large agglomeration, while its spherical shape was maintained. Accordingly, some conductor/insulator interfaces that forms between CoNi cores and SiO_2 shells disappear, which is supposed to decrease over-all conductor/insulator interface areas. On the other hand, the penetration of H_2 through SiO_2 shell to CoNi cores should be difficult as compared with TiO_2 shell (see TG data in Fig. S11 and associated discussion in Supporting Information), which then blocks the reduction of oxide or the elimination of defects. The improvement of conductivity can thus be limited during annealing, which is quite different from that in case of TiO_2 coating. The reduced interfaces area together with the restricted conductivity contributes to the decrease in the permittivity. The difference in microstructure evolution, either in the configuration or in the imperfect density, is responsible for the difference in the evolution of EM properties. Consequently, it can be inferred that TiO_2 coating would endow composite microspheres with better dielectric loss than SiO_2 coating.

The μ' of specimens containing CoNi microspheres as fillers presents an evident decrease from 2 to 7 GHz, and then slight fluctuation in the frequency range of 7–18 GHz, as illustrated in Fig. 6b. The μ'' exhibits a resonance peak at 5.1 GHz. This characteristic in permeability suggested the natural resonance of CoNi microspheres in the band[52–54]. Besides, the effects from eddy current can be hardly observed all through the band. Particles synthesized via solution chemical method usually have high resistivity, thus the eddy effect can be effectively suppressed. Therefore, the natural resonance is the main magnetic loss mechanism for CoNi microspheres. After TiO_2 coating, the permeability of CoNi@TiO_2 decreases slightly. The permeability of ferromagnetic particles basically depends on the M_s, thus the slight decrease in μ is ascribed to the reduction of M_s. Additionally, a distinct broad peak on μ'' curve at 15–16 GHz for CoNi@TiO_2 can be observed, which may be associated with the exchange resonance[55]. CoNi particles within local aggregations stacks very densely as intervals below 10 nm, which can be contributed to the exchange resonance. The permeability changes significantly after the fillers annealed, which can be distinguished from the plot shown in Fig. 6b. The μ' of annealed fillers increases in most frequency range, which is ascribed to the enhancement of M_s. The nature resonance frequency shifts to high frequency range of 8.4 GHz as identified from the μ'' curve, which would be significant to improve its EMA properties in the microwave range[56]. The presence of SiO_2 shell did not significantly influence permeability except a slight decrease, which can be distinguished from the plot shown in Fig. S10b.

From the above observations, it can suppose that the incorporation of dielectric TiO_2 and magnetic CoNi into the electromagnetic wave absorption system had generated massive dielectric and magnetic interactions at materials interfaces, which has a positive impact on the matching of permeability and permittivity[57]. Moreover, the effective complementarity between magnetic loss contributed by CoNi cores and dielectric loss from TiO_2 shells plays a vital role in the enhancement of electromagnetic wave absorption capability[58]. Therefore, it is possible to enhance the microwave absorption performance of core-shell structure microspheres.

The reflection loss (*RL*) of CoNi and CoNi@TiO_2 annealed microspheres are obtained according to the transmit line theory[39,59]. The results are shown in Fig. 7. It can be seen that the microspheres exhibit outstanding microwave absorption performance in terms of a thin absorber layer with a wide frequency bandwidth and strong

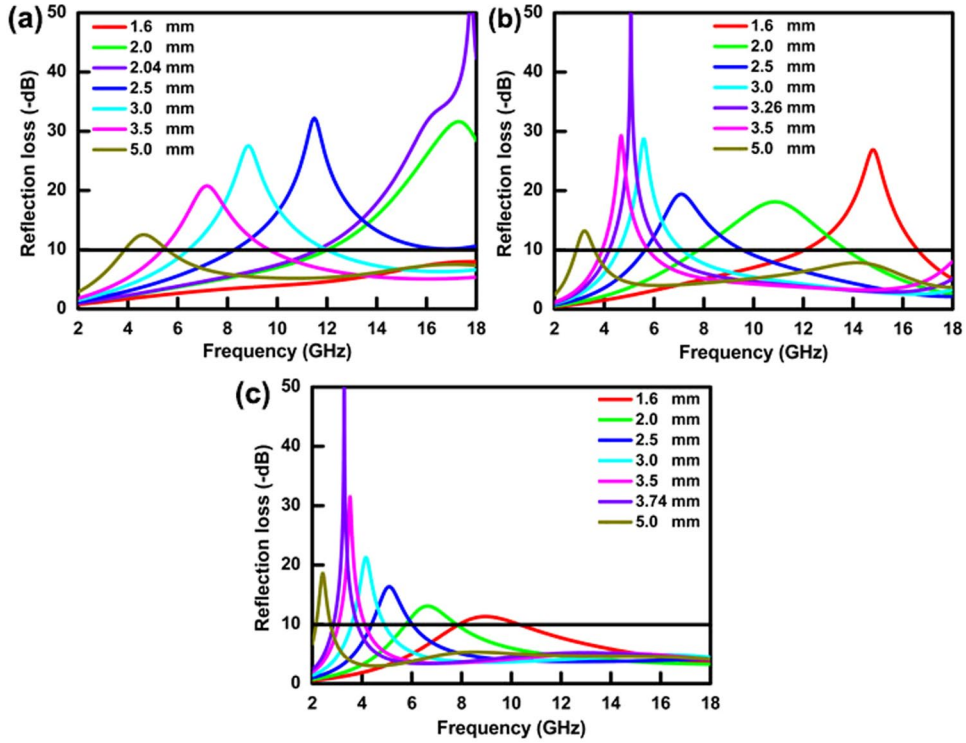

Figure 7. The frequency dependence of reflection loss of CoNi/paraffin composites. (**a**) CoNi microspheres; (**b**) CoNi@TiO_2 microspheres; (**c**) annealed CoNi@TiO_2 microspheres.

reflection loss. As shown in Fig. 7a, the maximum *RL* (RL_{max}) for coatings containing CoNi microspheres as fillers is 54.4 dB at 17.8 GHz with a matching thickness of 2.04 mm. Meanwhile, the absorption bandwidth with *RL* higher than 10 dB (EAB_{10}) is 6.2 GHz (11.8–18 GHz), covering the whole K_u band, which is technically significant for the application in K_u band. Moreover, an EAB_{10} of 9.6 GHz (8.4–18.0 GHz) is observed when a slightly increased matching thickness of 2.5 mm is applied, nearly covering the whole X-K_u (8–18 GHz) band. It can be supposed that the excellent microwave absorbing properties of CoNi microspheres is due to its novel conical bulges structure. The surface architecture is an important factor that can tune the microwave absorption capability. The conical bulges on the CoNi microsphere surfaces should have great impacts on the electromagnetic wave absorption performance. The incident electromagnetic wave might suffer multiple scattering in the space among the conical bulges, leading to more intense exhaustion and absorption. Additionally, the large exposed conical bulges would cause strong interfacial magnetic dipole polarization[60], which may further improve electromagnetic absorption.

The CoNi@TiO_2 composite microspheres display high EMA properties referring to both the maximum *RL* and the absorption frequency band, as shown in Fig. 7b. RL_{max} of 59.2 dB was obtained at 5.07 GHz in a coating of 3.26 mm. *RL* higher than 5 dB is 5.8 GHz (3.5–9.3 GHz), covering the whole C band (4–8 GHz). Specifically, *RL* higher than 5 dB of 9.1 GHz is achieved in 4.5–13.6 GHz band when a matching thickness of 2.5 mm is applied. Meanwhile, coating with thickness of 1.6 mm presents *RL* higher than 5 dB of 10.5 GHz in 7.5–18.0 GHz band, covering C, X and K_u band, or an EAB_{10} of 4.6 GHz in 12.0–16.6 GHz band. It can be seen that the absorption band would shift to much lower frequency if annealed fillers are used, as shown in Fig. 7c. RL_{max} of 76.6 dB at 3.3 GHz with a thickness of 3.74 mm is obtained, and an absorption bandwidth ($RL > 5$ dB) is 2.3 GHz (2.4–4.6 GHz), nearly covering the whole S band (2–4 GHz). These results indicate that excellent EMA performances can be obtained in S band. Moreover, the absorption bandwidth with *RL* higher than 5 dB is 9.1 GHz in 6.0–15.1 GHz with a thickness of 1.6 mm.

Compared with CoNi@TiO_2 coating, excellent EMA performance also can be obtained using CoNi@SiO_2 as fillers. The RL_{max} is 65.6 dB in 9.2 GHz, and an EAB_{10} is 5.5 GHz (6.7–12.2 GHz) with a thickness of 2.75 mm, as described in Fig. S12a. However, the microwave absorption capability slightly declines both in reflection loss and in effective absorption bandwidth of CoNi@SiO_2 annealed fillers (Fig. S12b). Meanwhile, the absorption band shifts to higher frequency. As described in Fig. S12b, RL_{max} is 73.8 dB at 17.7 GHz and the EAB_{10} is 3.3 GHz from 14.7 to 18.0 GHz with a thickness of 1.82 mm. When the thickness is 1.6 mm, the absorption bandwidth (*RL* higher than 5 dB) is 4.6 GHz (13.4–18.0 GHz), which is much narrower than that of CoNi@TiO_2 annealed microspheres. From the RL_{max} curves in Fig. S12c, it can be found that the absorption peaks shift obviously after the introduction of TiO_2 shells. Upon TiO_2 coating, microwave absorption moves to S band, indicating excellent EMA performances in these bands. Nevertheless, microwave absorption remains in K_u band after SiO_2 coating. All results indicate that coating of TiO_2 broadens absorption bandwidth and obtains selective-frequency absorption, demonstrating that construction of core-shell structure is an efficient strategy to improve EMA and tailor

strong absorption bands. Table S1 shows the typical CoNi-based composites and their corresponding microwave absorption performances in recent literatures. According to the comparison, the composite microspheres in our study are more competitive than other microwave absorbers for EMA applications in terms of thin thickness and wide frequency range.

Conclusions

In summary, CoNi microspheres with conical bulges were successfully synthesized via a simple liquid-phase reduction method. CoNi@TiO_2 core-shell microspheres with prominently enhanced microwave absorption performance were constructed via sol-gel process. Compared with bare CoNi and annealed CoNi@SiO_2, annealed CoNi@TiO_2 microspheres display superior microwave absorption performance with RL_{max} up to 76.6 dB, and the absorption bandwidth of 1.2 GHz in S band. Additionally, the absorption bandwidth ($RL > 5$ dB) can be broaden to 9.1 GHz with a thin thickness of 1.6 mm. The superior EMA properties of CoNi@TiO_2 core-shell microspheres derive from the intense dielectric loss and magnetic loss. The TiO_2 shells together with the annealing on one hand ensure CoNi microspheres effective isolation, on the other hand, induce enhanced interfacial polarization and strong dipole polarization to improve the dielectric loss. CoNi@TiO_2 microspheres demonstrate their excellence on account of the combination of strong magnetic loss from CoNi cores and excellent dielectric loss from TiO_2 shells. These results ensure that the microspheres in our study with merits of strong absorption and broad effective absorption bandwidths are greatly superior to other CoNi-based EMA fillers. Thus, it is believed that the composites can be used as a promising candidate for high-performance microwave absorbers.

Methods

All chemicals were of analytical grade and used directly without any pre-treatment. Nickel chloride hexahydrate ($NiCl_2{\cdot}6H_2O$), cobalt chloride hexahydrate ($CoCl_2{\cdot}6H_2O$), ethylene glycol (EG), sodium hydroxide (NaOH), hydrazine hydrate ($N_2H_4{\cdot}H_2O$, 85%), ammonium hydroxide solution (28 wt%), tetraethyl orthosilicate (TEOS), tetrabutyl orthotitanate (TBOT), acetonitrile and ethanol were all purchased from Sinopharm Chemical Reagent Company.

Preparation of CoNi microspheres. CoNi spheres were synthesized by a liquid phase reduction process. Typically, 0.01 mol of $NiCl_2{\cdot}6H_2O$ and 0.01 mol of $CoCl_2{\cdot}6H_2O$ were dissolved in 200 mL of EG under mechanical stirring at 85 °C, followed by the addition of 0.12 mol of NaOH. After 20 min, 8 mL of $N_2H_4{\cdot}H_2O$ was added. The reaction duration is 1 h. The obtained products were washed for several times with distilled water and absolute ethanol. Finally, the products were dried in a vacuum oven at 60 °C overnight for further characterization.

Preparation of CoNi@TiO_2 microspheres. 0.5 g of as-prepared CoNi microspheres were dispersed in the mixture solvent containing ethanol (180 mL) and acetonitrile (60 mL). The mixture was ultrasonicated for 30 min, followed by the addition of 1 mL of ammonia aqueous solution under mechanical stirring. Afterward, 0.5 mL of TBOT was added, and the reaction was allowed to proceed for another 2 h. The black particles were collected and washed with ethanol, and then dried at 60 °C.

Preparation of CoNi@SiO_2 microspheres. 0.5 g of CoNi microspheres were dispersed in ethanol (160 mL) and deionized water (40 mL), and sonicated for 30 min. Then, 4 mL of ammonia aqueous solution was added under mechanical stirring. Afterward, 0.2 mL of TEOS was added, and the reaction was allowed to occur for 4 h. The resulted precipitates were collected and washed with absolute ethanol, and dried at 60 °C. The as-prepared CoNi@TiO_2 and CoNi@SiO_2 microspheres were annealed at 600 °C for 2 h under H_2 atmosphere for microstructure tailoring.

Characterization. The crystal structure of as-prepared products was characterized by X-ray diffraction (XRD, Rigaku D/max-rB, Cu K_α). The morphologies of microspheres were characterized using a field-emission scanning electron microscope (SEM, FEI Quanta 200 F) equipped with an energy dispersive spectrometer (EDS), and a transmission electron microscope (TEM, JEOL JEM-2100). The element values in the samples were analyzed on X-ray photoelectron spectroscopy (XPS, Thermo Fisher Scientific VG K_α Probe) using Al K_α radiation as the excitation source. The magnetic properties of the powder samples were measured by a vibrating sample magnetometer (VSM, Lakeshore 7300) at room temperature. The permittivity and permeability of samples in 2–18 GHz range were examined with a vector network analyzer (VNA, Agilent N5230A). For testing, 70 wt.% CoNi particles were homogeneously dispersed in paraffin matrix. Thermogravimetry curves of composite microspheres were recorded on a thermal gravimetric analyzer (TG, SDT Q600 V20.9 Build 20) under air from room temperature to 800 °C with a ramping rate of 10 °C min^{-1}.

References

1. Kong, L. *et al*. Macroscopic bioinspired graphene sponge modified with *in-situ* grown carbon nanowires and its electromagnetic properties. *Carbon* **111**, 94–102 (2017).
2. Jiang, L. W. *et al*. Carbon-encapsulated Fe nanoparticles embedded in organic polypyrrole polymer as a high performance microwave absorber. *J. Phys. Chem. C* **120**, 28320–28329 (2016).
3. Zeng, Q. *et al*. Air@rGO€Fe_3O_4 microspheres with spongy shells: self-assembly and microwave absorption performance. *J. Mater. Chem. C* **4**, 10518–10528 (2016).
4. Liu, P. J., Yao, Z. J., Zhou, J. T., Yang, Z. H. & Kong, L. B. Small magnetic Co-doped NiZn ferrite/graphene nanocomposites and their dual-region microwave absorption performance. *J. Mater. Chem. C* **4**, 9738–9749 (2016).
5. Qi, X. S. *et al*. Heteronanostructured Co@carbon nanotubes-graphene ternary hybrids: synthesis, electromagnetic and excellent microwave absorption properties. *Sci. Rep.* **6**, 37972 (2016).
6. Zhan, L. L. *et al*. Facile synthesis of iron oxides/reduced graphene oxide composites: application for electromagnetic wave absorption at high temperature. *Sci. Rep.* **5**, 9298 (2015).

7. Ding, Y. *et al*. Reduced graphene oxide functionalized with cobalt ferrite nanocomposites for enhanced efficient and lightweight electromagnetic wave absorption. *Sci. Rep.* **6**, 32381 (2016).
8. Sun, G. B., Dong, B. X., Cao, M. H., Wei, B. Q. & Hu, C. W. Hierarchical dendrite-like magnetic materials of Fe_3O_4, γ-Fe_2O_3, and Fe with high performance of microwave absorption. *Chem. Mater.* **23**, 1587–1593 (2011).
9. Zhao, B. *et al*. Yolk-shell Ni@SnO_2 composites with a designable interspace to improve electromagnetic wave absorption properties. *ACS Appl. Mater. Interfaces* **8**, 28917–28925 (2016).
10. Xu, C., Nie, D., Chen, H., Wang, Y. & Liu, Y. Template-free synthesis of magnetic CoNi nanoparticles via a solvothermal method. *Mater. Lett.* **138**, 158–161 (2015).
11. Feng, J. *et al*. Interfacial interactions and synergistic effect of CoNi nanocrystals and nitrogen-doped graphene in a composite microwave absorber. *Carbon* **104**, 214–225 (2016).
12. Liu, Q. *et al*. Dependency of magnetic microwave absorption on surface architecture of $Co_{20}Ni_{80}$ hierarchical structures studied by electron holography. *Nanoscale* **7**, 1736–1743 (2015).
13. Guo, X. Q., Bai, Z. Y., Zhao, B., Zhang, R. & Chen, J. B. Microwave absorption properties of CoNi nanoparticles anchored on the reduced grapheme oxide. *J. Mater. Sci.: Mater. Electron.* **27**, 8408–8415 (2016).
14. Li, H. *et al*. Hollow CoNi alloy submicrospheres consisting of CoNi nanoplatelets: facile synthesis and magnetic properties. *Mater. Lett.* **67**, 346–348 (2012).
15. Rashid, M. H., Raula, M. & Mandal, T. K. Polymer assisted synthesis of chain-like cobalt-nickel alloy nanostructures: magnetically recoverable and reusable catalysts with high activities. *J. Mater. Chem.* **21**, 4904–4917 (2011).
16. Ming, W., Wu, Q., Jin, P., Wu, Q. & Wang, C. Fabrication of Pt-loaded NiCo nanochains with superior catalytic dehydrogenation activity. *J. Colloid Interface Sci.* **416**, 220–226 (2014).
17. Rosa, W. O., Vivas, L. G., Pirota, K. R., Asenjo, A. & Vázquez, M. Influence of aspect ratio and anisotropy distribution in ordered CoNi nanowire arrays. *J. Magn. Magn. Mater.* **324**, 3679–3682 (2012).
18. Pereira, A. *et al*. Tailoring the magnetic properties of ordered 50-nm-diameter CoNi nanowire arrays. *J. Nanopart. Res.* **15**, 2041 (2013).
19. Pan, S., An, Z., Zhang, J. & Song, G. Synthesis and hierarchical assembly of CoNi flowery particles. *Mater. Chem. Phys.* **124**, 342–346 (2010).
20. Khorsand, S., Raeissi, K., Ashrafizadeh, F. & Arenas, M. A. Super-hydrophobic nickel-cobalt alloy coating with micro-nano flower-like structure. *Chem. Eng. J.* **273**, 638–646 (2015).
21. Rafique, M. Y. *et al*. Controlled synthesis, phase formation, growth mechanism, and magnetic properties of 3-D CoNi alloy microstructures composed of nanorods. *CrystEngComm* **15**, 5314–5325 (2013).
22. Xu, Q., Wang, Z.-J., Wang, Y.-G. & Sun, H.-Y. The effect of Co content on the structure and the magnetic properties of Co_xNi_{1-x} nanotubes. *J. Magn. Magn. Mater.* **419**, 166–170 (2016).
23. Zhang, H.-M., Zhang, X.-L., Zhang, J.-J., Li, Z.-Y. & Sun, H.-Y. Fabrication and magnetic properties of CoNi alloy nanotube arrays. *J. Magn. Magn. Mater.* **342**, 69–73 (2013).
24. Li, H. *et al*. Controlled synthesis of three-dimensional CoNi microstructures composed of single crystal CoNi nanoleaves. *CrystEngComm* **14**, 2974–2980 (2012).
25. Liu, T., Pang, Y., Zhu, M. & Kobayashi, S. Microporous Co@CoO nanoparticles with superior microwave absorption properties. *Nanoscale* **6**, 2447–2454 (2013).
26. Wang, Z. *et al*. Magnetic and microwave absorption properties of self-assemblies composed of core-shell cobalt-cobalt oxide nanocrystals. *Phys. Chem. Chem. Phys.* **17**, 3796–3801 (2015).
27. Liu, X., Geng, D., Meng, H., Shang, P. & Zhang, Z. Microwave-absorption properties of ZnO-coated iron nanocapsules. *Appl. Phys. Lett.* **92**, 173117 (2008).
28. Wang, L., Xing, H., Gao, S., Ji, X. & Shen, Z. Porous flower-like NiO@graphene composites with superior microwave absorption properties. *J. Mater. Chem. C* **5**, 2005–2014 (2017).
29. You, W., Bi, H., She, W., Zhang, Y. & Che, R. Dipolar-distribution cavity γ-Fe_2O_3@C@α-MnO_2 nanospindle with broadened microwave absorption bandwidth by chemically etching. *Small* **13**, 1602779 (2017).
30. Ren, Y. L. *et al*. Quaternary nanocomposites consisting of graphene, Fe_3O_4@Fe core@shell, and ZnO nanoparticles: synthesis and excellent electromagnetic absorption properties. *ACS Appl. Mater. Interfaces* **4**, 6436–6442 (2012).
31. Zhu, J. H., Wei, S. Y., Haldolaarachchige, N., Young, D. P. & Guo, Z. H. Electromagnetic field shielding polyurethane nanocomposites reinforced with core-shell Fe-silica nanoparticles. *J. Phys. Chem. C* **115**, 15304–15310 (2011).
32. Zhao, B. *et al*. Facile preparation and enhanced microwave absorption properties of core-shell composite spheres composited of Ni cores and TiO_2 shells. *Phys. Chem. Chem. Phys.* **17**, 8802–8810 (2015).
33. Ren, Y. L. *et al*. Three-dimensional SiO_2@Fe_3O_4 core/shell nanorod array/graphene architecture: synthesis and electromagnetic absorption properties. *Nanoscale* **5**, 12296–12303 (2013).
34. Li, X. H. *et al*. One-pot synthesis of $CoFe_2O_4$/graphene oxide hybrids and their conversion into FeCo/graphene hybrids for lightweight and highly efficient microwave absorber. *J. Mater. Chem. A* **3**, 5535–5546 (2015).
35. Li, H. *et al*. Mesoporous titania spheres with tunable chamber stucture and enhanced photocatalytic activity. *J. Am. Chem. Soc.* **129**, 8406–8407 (2007).
36. Xia, T., Zhang, C., Oyler, N. A. & Chen, X. Hydrogenated TiO_2 nanocrystals: a novel microwave absorbing material. *Adv. Mater.* **25**, 6905–6910 (2013).
37. Zarifi, M. H., Farsinezhad, S., Abdolrazzaghi, M., Daneshmand, M. & Shankar, K. Selective microwave sensors exploiting the interaction of analytes with trap states in TiO_2 nanotube arrays. *Nanoscale* **8**, 7466–7473 (2016).
38. Chen, C. *et al*. Fabrication of hierarchical TiO_2 coated $Co_{20}Ni_{80}$ particles with tunable core sizes as high-performance wide-band microwave absorbers. *Phys. Chem. Chem. Phys.* **18**, 26712–26718 (2016).
39. Liu, J. *et al*. Microwave absorption enhancement of multifunctional composite microspheres with spinel Fe_3O_4 cores and anatase TiO_2 shells. *Small* **8**, 1214–1221 (2012).
40. Matsumoto, Y. *et al*. Room-temperature ferromagnetism in transparent transition metal-doped titanium dioxide. *Science* **291**, 854–856 (2001).
41. Xu, C., Nie, D., Chen, H., Wang, Y. & Liu, Y. Solvothermal synthesis of cauliflower-like CoNi microstructures with enhanced magnetic property. *Mater. Lett.* **142**, 246–249 (2015).
42. Chen, N. *et al*. Co_7Fe_3 and Co_7Fe_3@SiO_2 nanospheres with tunable diameters for high-performance electromagnetic wave absorption. *ACS Appl. Mater. Interfaces* **9**, 21933–21941 (2017).
43. Bulut, A. *et al*. Carbon dispersed copper-cobalt alloy nanoparticles: a cost-effective heterogeneous catalyst with exceptional performance in the hydrolytic dehydrogenation of ammonia-borane. *Appl. Catal. B* **180**, 121–129 (2016).
44. Liu, Q., Zhang, D. & Fan, T. Electromagnetic wave absorption properties of porous carbon/Co nanocomposites. *Appl. Phys. Lett.* **93**, 013110 (2008).
45. Castel, V. & Brosseau, C. Magnetic field dependence of the effective permittivity in $BaTiO_3$/Ni nanocomposites observed via microwave spectroscopy. *Appl. Phys. Lett.* **92**, 233110 (2008).
46. Xu, H. *et al*. Carbon hollow microspheres with a designable mesoporous shell for high-performance electromagnetic wave absorption. *ACS Appl. Mater. Interfaces* **9**, 6332–6341 (2017).

47. Lv, H. L. *et al*. Co_xFe_y@C composites with tunable atomic ratios for excellent electromagnetic absorption properties. *Sci. Rep.* **5**, 18249 (2015).
48. Lagarkov, A. & Sarychev, A. Electromagnetic properties of composites containing elongated conducting inclusions. *Phys. Rev. B* **53**, 6318 (1996).
49. Wen, S., Liu, Y. & Zhao, X. Effect of annealing on electromagnetic performance and microwave absorption of spherical cobalt particles. *J. Phys. D: Appl. Phys.* **48**, 405001 (2015).
50. Feng, J., Hou, Y., Wang, Y. & Li, L. Synthesis of hierarchical $ZnFe_2O_4$@SiO_2@RGO core-shell microspheres for enhanced electromagnetic wave absorption. *ACS Appl. Mater. Interfaces* **9**, 14103–14111 (2017).
51. Wen, B. *et al*. Temperature dependent microwave attenuation behavior for carbon-nanotube/silica composites. *Carbon* **65**, 124–139 (2013).
52. Wang, H. *et al*. Broadband microwave absorption of CoNi@C nanocapsules enhanced by dual dielectric relaxation and multiple magnetic resonances. *Appl. Phys. Lett.* **102**, 223113 (2013).
53. Ma, F., Qin, Y. & Li, Y.-Z. Enhanced microwave performance of cobalt nanoflakes with strong shape anisotropy. *Appl. Phys. Lett.* **96**, 202507 (2010).
54. Ma, J., Li, J., Ni, X. & Zhang, X. Microwave resonance in Fe/SiO_2 nanocomposite. *Appl. Phys. Lett.* **95**, 102505 (2009).
55. Toneguzzo, P., Acher, O., Viau, G., Fievet-Vincent, F. & Fievet, F. Observations of exchange resonance modes on submicrometer sized ferromagnetic particles. *J. Appl. Phys.* **81**, 5546–5548 (1997).
56. Zhang, X. *et al*. Microwave absorption properties of the carbon-coated nickel nanocapsules. *Appl. Phys. Lett.* **89**, 053115 (2006).
57. Liu, Q. *et al*. CoNi@SiO_2@TiO_2 and CoNi@Air@TiO_2 microspheres with strong wideband microwave absorption. *Adv. Mater.* **28**, 486–490 (2016).
58. Hu, Q. *et al*. Preparation of porous Fe_2O_3 nanorods-reduced graphene oxide nanohybrids and their excellent microwave absorption properties. *Sci. Rep.* **7**, 11213 (2017).
59. Che, R., Peng, L. M., Duan, X. F., Chen, Q. & Liang, X. Microwave absorption enhancement and complex permittivity and permeability of Fe encapsulated within carbon nanotubes. *Adv. Mater.* **16**, 401–405 (2004).
60. Che, R., Peng, L. M., Duan, X. F., Chen, Q. & Liang, X. Insights into size-dominant magnetic microwave absorption properties of CoNi microflowers via off-axis electron holography. *ACS Appl. Mater. Interfaces* **7**, 4233–4240 (2015).

Acknowledgements

This work was financially supported by the National Natural Science Foundation of China (Grant no. 51201048).

Author Contributions

N.C., J.-T.J. and L.Z. conceived and designed the experiments. N.C. performed the experiments. S.-J.Y contributed to measure magnetic performance. All authors discussed the results and N.C., C.-Y.X., J.-T.J contributed to the manuscript preparation. All authors reviewed the manuscript.

Additional Information

Supplementary information accompanies this paper at https://doi.org/10.1038/s41598-018-21047-z.

Competing Interests: The authors declare no competing interests.

Publisher's note: Springer Nature remains neutral with regard to jurisdictional claims in published maps and institutional affiliations.